





# Establishing an objective biomarker for corneal cystinosis using a threshold-based Spectral domain optical coherence tomography imaging algorithm

Leonie Keidel,<sup>1</sup>  Carolin Elhardt,<sup>1</sup>  Katharina Hohenfellner,<sup>2</sup> Siegfried Priglinger,<sup>1</sup> Benedikt Schworm,<sup>1</sup>  Christian Wertheimer,<sup>1</sup>  Claudia Priglinger<sup>1</sup> and Nikolaus Luft<sup>1</sup>

<sup>1</sup>Department of Ophthalmology, Ludwig-Maximilians-University, Munich, Germany

<sup>2</sup>Department of Pediatric Nephrology, RoMed Klinikum Rosenheim, Rosenheim, Germany

## ABSTRACT.

**Purpose:** The purpose of the present study was to establish a semi-automated threshold-based image segmentation algorithm to detect and objectively quantify corneal cystine crystal deposition in ocular cystinosis with anterior segment optical coherence tomography (AS-OCT).

**Methods:** This prospective, observational, comparative study included 88 eyes of 45 patients from the German Cystinosis Registry Study as well as 68 eyes of 35 healthy control subjects. All eyes were imaged with AS-OCT (Cirrus HD-OCT 5000, Carl Zeiss Meditec AG, Jena, Germany). As an initial step, B-scan images were subjectively analysed for typical changes in morphology in comparison to healthy controls. Based on the experience gained, an objective semi-automated B-scan image segmentation algorithm was developed using a grey scale value-based threshold method to automatically quantify corneal crystals.

**Results:** On AS-OCT B-scans, corneal crystals appeared as hyperreflective deposits within the corneal stroma. The crystals were distributed either in all stromal layers (43 eyes, 49%) or confined to the anterior (23 eyes, 26%) or posterior stroma (22 eyes, 25%), respectively. The novel automatic B-scan image segmentation algorithm was most efficient in delineating corneal crystals at higher grey scale thresholds (e.g. 226 of a maximum of 255). Significant differences in suprathreshold grey scale pixels were observable between cystinosis patients and healthy controls ( $p < 0.001$ ). In addition, the algorithm was able to detect an age-dependent depth distribution profile of crystal deposition.

**Conclusion:** Objective quantification of corneal cystine crystal deposition is feasible with AS-OCT and can serve as a novel biomarker for ocular disease control and topical treatment monitoring.

**Key words:** biomarker – cornea – cystine crystals – cystinosis – greyscale – image segmentation algorithm – optical coherence tomography

†First authors contributed equally to this work.

‡German Cystinosis Study Group: S Bechtold Dalla Pozza, C Bergmann, M Buss, R Dosch, J Erler, T Getzinger, N Herzig, K Hohenfellner, H Holla, C Knerr, C Koepl, C Ockert, M Passow, J Rohayem, G Steidle, A Thiele, U Treikauskas, K Vill, R Weber, D Weitzel

Acta Ophthalmol. 2021; 99: e189–e195

© 2020 The Authors. Acta Ophthalmologica published by John Wiley & Sons Ltd on behalf of Acta Ophthalmologica Scandinavica Foundation

This is an open access article under the terms of the Creative Commons Attribution License, which permits use, distribution and reproduction in any medium, provided the original work is properly cited.

doi: 10.1111/aos.14569

## Introduction

Nephropathic cystinosis is a rare autosomal recessive lysosomal storage disease caused by biallelic mutations in the *CTNS* gene, which encodes a protein (cystinosin) that transports cystine out of lysosomes (Gahl et al. 1982; Town et al. 1998; Kalatzis & Antignac 2003; David et al. 2019). Lysosomal storage of cystine damages several organs and different ophthalmic structures, including the cornea (Gahl et al. 2002). A small free thiol, cysteamine, depletes cells of cystine and has protective effects on renal function, growth and nonrenal complications, when administered orally (Thoene et al. 1976; Gahl et al. 1987; Gahl et al. 1992; Nesterova & Gahl 2008). In contrast, corneal crystal deposition is only amenable to topical cysteamine-containing eyedrops (Cantani et al. 1983; Tsilou et al. 2007). In several studies topical cysteamine treatment has proven effective in partially dissolving corneal crystals (Kaiser-Kupfer et al. 1987; Bradbury et al. 1991; Jones et al. 1991; Graf et al. 1992; Blanksma et al. 1996; Gahl et al. 2000). Early diagnosis and management of the ocular manifestations of infantile nephropathic cystinosis are essential as early initiation of and adherence to topical therapy has significant impact on disease progression (Nesterova & Gahl 2013). Thus, monitoring the effect of topical therapy, which is often

hampered by poor patient adherence – especially in paediatric cystinosis – is paramount.

Gahl et al. (2000) showed that vision-impairing corneal crystal accumulation as quantified by the corneal cystine crystal score – a clinical score based on digital slit lamp photography – can be markedly reduced by the constant administration of cysteamine-containing eyedrops. However, corneal cystine crystals, which have been found to deposit predominantly in the anterior corneal stromal lamellae (Kalatzis et al. 2007), cause distinct dysphotopsia due to scattering of incoming visible light (Kaiser-Kupfer et al. 1986). Patients suffer from severe photophobia that can entail severe and irreversible blepharospasm (Gahl et al. 2000), thereby impeding standardized acquisition of digital photographs as well as accurate quantification of crystals by slit lamp examination. Furthermore, interpretation of the slit lamp photographs relies on subjective judgment rather than on objective criteria and may thus bear a potential for inter-investigator variabilities.

Besides slit lamp biomicroscopy, *in vivo* confocal microscopy (IVCM) appears to be a sensitive imaging technique to detect corneal cystine crystal deposition (Simpson et al. 2011a; Simpson et al. 2011b). This optical technique, however, is limited by its time-consuming and highly operator-dependent nature, requires direct contact with the ocular surface and operates in the visible light spectrum. Especially in severely photophobic as well as in paediatric patients, a non-contact imaging method independent of visible light would be desirable.

Anterior segment optical coherence tomography (AS-OCT) is a noncontact imaging modality that enables cross-sectional images of the corneal tissue in a near histological resolution (Han et al. 2016). As AS-OCT operates in the infrared spectrum invisible for the human eye, this technique seems particularly suitable for cystinosis patients. To date, corneal cystine crystals, which present as hyperreflective punctuate foci on AS-OCT (Labbe et al. 2009), have only been manually analysed regarding their depth distribution on AS-OCT B-scans using digital callipers (Liang et al. 2015). As of today, however, no objective methods are available for precise grading and monitoring of corneal cystinosis using this promising imaging technique.

Hence, the aim of the present study was to develop and validate a semi-automated AS-OCT based imaging algorithm for objective characterization and monitoring of corneal cystine crystal deposition patterns in infantile nephropathic cystinosis.

## Materials and Methods

This prospective comparison study recruited patients with infantile nephropathic cystinosis from the German Cystinosis Registry Study carried out by the Interdisciplinary Cystinosis Clinic Rosenheim as well as healthy control subjects between 2018 and 2019. The German Cystinosis Registry exclusively includes patients with a genetically confirmed diagnosis of cystinosis independent of age. Eyes with previous corneal surgery or injury were excluded from the trial. All research and measurements followed the tenets of the Declaration of Helsinki. Ethics committee approval for this study was waived by the ethics committee (Ethics Committee of the Bavarian Medical Association; 11th March 2015) on the basis that the planned project of an interdisciplinary cystinosis-database does not fall under the consultation obligation according to paragraph 15 of the professional code of conduct for physicians in Bavaria, Germany. Consent to use their data for analysis and scientific publication was obtained from all participating patients. Ethics committee approval for the AS-OCT imaging of healthy control subjects had been obtained from the local ethics committee of the Ludwig-Maximilians University as part of a prior study on healthy volunteers conducted at our institution (study registration number 508/14).

### Clinical examinations

All patients underwent a complete ophthalmological examination comprising slit-lamp biomicroscopy. Subjective manifest refraction was measured using the Jackson cross-cylinder method. Monocular best-corrected distance visual acuity (CDVA) was determined using standard ETDRS charts at 4 m.

### Anterior segment optical coherence tomography

Standardized AS-OCT imaging was performed with the Zeiss Cirrus HD-OCT 5000 (Carl Zeiss Meditec AG; Oberkochen, Germany) with an axial resolution of 4  $\mu\text{m}$ . For each patient, one singular 9.0 mm horizontal and one singular 9.0 mm vertical paracentral B-scan was acquired in a standardized manner. Utmost care was taken to obtain the scans most adjacent to but completely excluding the central vertex reflex artefacts. For subsequent digital image analysis, the higher quality scan was selected according to the subjective judgment of two expert AS-OCT readers.

### Subjective and manual AS-OCT image analysis

As a first step, pathological changes on B-scan images of cystinosis patients were subjectively described in comparison to scans of the healthy control group. Moreover, the thickness of the central cornea and the central corneal stroma was determined by two independent examiners using the digital calliper instrument in ImageJ (ImageJ 1.52; National Institutes of Health, Bethesda, Maryland, USA; Fig. 1). Accordingly, the depth distribution of

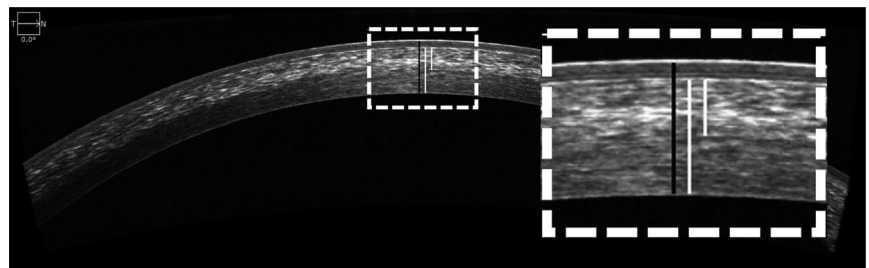


**Fig. 1.** Corneal sublayer thickness and crystal depth distribution measurements using digital callipers. The black calliper shows the measurement of central corneal thickness. The long white calliper measures the central corneal stromal thickness and the short white calliper quantifies the depth of crystals posterior to Bowman's layer as subjectively measured by the examiners. (Digitally enlarged area: 3 $\times$  of original).

corneal crystals was subjectively determined by two independent examiners by drawing the same digital calliper from Bowman's layer to the most posterior presentation of corneal crystals. For all subjective calliper measurements, the means of both measurements as well as the squared inter-rater Pearson correlation coefficient ( $R^2$ ) were calculated. In addition, the results were analysed for four different age groups ( $\leq 10$ ; 11–20; 21–30;  $>30$  years).

**Objective, semi-automated AS-OCT image segmentation**

The AS-OCT images present with 256 different shades of grey for image display with 0 corresponding to the colour black as the darkest value and 255 to the colour white as the brightest value. Hyperreflective structures of the cornea can be semi-automatically segmented by using grey scale values as thresholds and quantifying all pixels that present brighter than a respective threshold value. For that purpose, in ImageJ, a rectangular region of interest (ROI) of 100 pixels horizontally and the individual stromal thickness vertically was manually placed within the stroma of the central B-scan area (Fig. 2). Great care was taken to align the ROI horizontally with the highest point of the cornea and to fit the ROI completely within the stromal area, thereby consistently avoiding the hyperreflective interface with Bowman's layer. A total of 16 different grey scale thresholds (at every 16 grey scale values) were applied to find an optimal threshold for discriminating between corneal crystals in cystinosis patients and physiologic hyperreflective stromal structures in healthy corneas. To account for the interindividual variability in cornea stromal pachymetry

and, hence, the height and total area of the ROI, the number of pixels above the respective threshold was calculated as a percentage of the total pixel count within an individual's entire ROI.

**Crystal depth distribution patterns**

In order to objectively characterize crystal depth distribution, the previously described rectangular ROI was subdivided in three equally sized rectangular segments representative of the anterior, mid and posterior corneal stroma, respectively. The number of pixels surpassing the respective grey scale value threshold in each of the three segments was calculated as the percentage of the total number of suprathreshold pixels of the entire ROI.

**Statistical analysis**

All statistical analysis was performed using Excel 365 (Microsoft Corporation; Redmond, WA, USA) and SPSS Statistics Version 25.0 (IBM; Armonk, NY, USA). All graphs were plotted using Graph Pad Prism 8 (GraphPad Software, San Diego, CA, USA). All data are presented as mean  $\pm$  SD. Box plots show the mean and the 95% confidence interval. Normality of data was confirmed using histogram frequency analysis and the Shapiro Wilk test. Statistical comparison between experimental groups was carried out using an ANOVA with a Bonferroni post hoc test in more than two groups and by independent samples t-test if two groups were compared. Linear regression analyses were performed to correlate CDVA with suprathreshold pixels as percentages of the pixel counts of the entire ROI. The inter-rater correlation was evaluated by the squared Pearson

correlation coefficient ( $R^2$ ). For all analyses, a p-value of  $<0.05$  was considered as an indicator of statistical significance.

**Results**

**Patient characteristics**

The cystinosis group included 88 eyes of 45 patients with a male to female ratio of 46:42 and a mean age of  $21.1 \pm 12.2$  years. The healthy control group consisted of 68 eyes of 35 patients with a male to female ratio of 35:33 and a mean age of  $27.8 \pm 10.1$  years. Table 1 shows the distribution of subjects in different age groups.

**Subjective and manual AS-OCT image analysis**

Subjectively, the only difference between B-scans of cystinosis patients and healthy controls were hyperreflective punctuate or plane hyperreflective deposits within the corneal stroma of the former group (Fig. 3). Distinct crystal distribution patterns were observable: a total of 43 (49%) eyes showed crystals distributed homogeneously in all stromal layers (Fig. 3A), 23 (26%) eyes predominantly in the anterior stroma (Fig. 3B) and 22 (25%) eyes predominantly in the posterior stroma with less densely scattered crystals in the anterior and mid stroma (Fig. 3C).

With respect to the digital calliper measurements, all calculated inter-rater correlation coefficients ( $R^2$ ) were 0.82 or higher (Table 2). Corneal and stromal thickness measurements showed

**Table 1.** Subjects' age groups.

	Cystinosis patients (mean $\pm$ SD)	Control group (mean $\pm$ SD)
No. of eyes ( <i>n</i> )	88	68
No. of patients ( <i>n</i> )	45	35
Gender (m/f)	23 m/22 f	18 m/17 f
Mean age (years)	$21.1 \pm 12.2$	$27.8 \pm 10.1$
Age distribution (years)		
$\leq 10$	8	0
11–20	17	8
21–30	13	19
$>30$	7	8

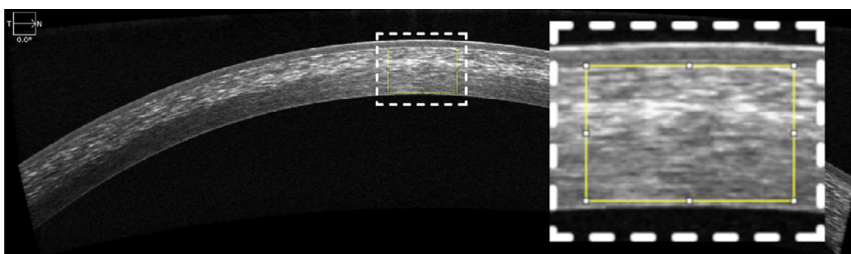


**Fig. 2.** The region of interest (ROI) was chosen to be 100 pixels horizontally and the individual stromal thickness vertically in the corneal centre (yellow box). (Digitally enlarged area: 3 $\times$  of original).

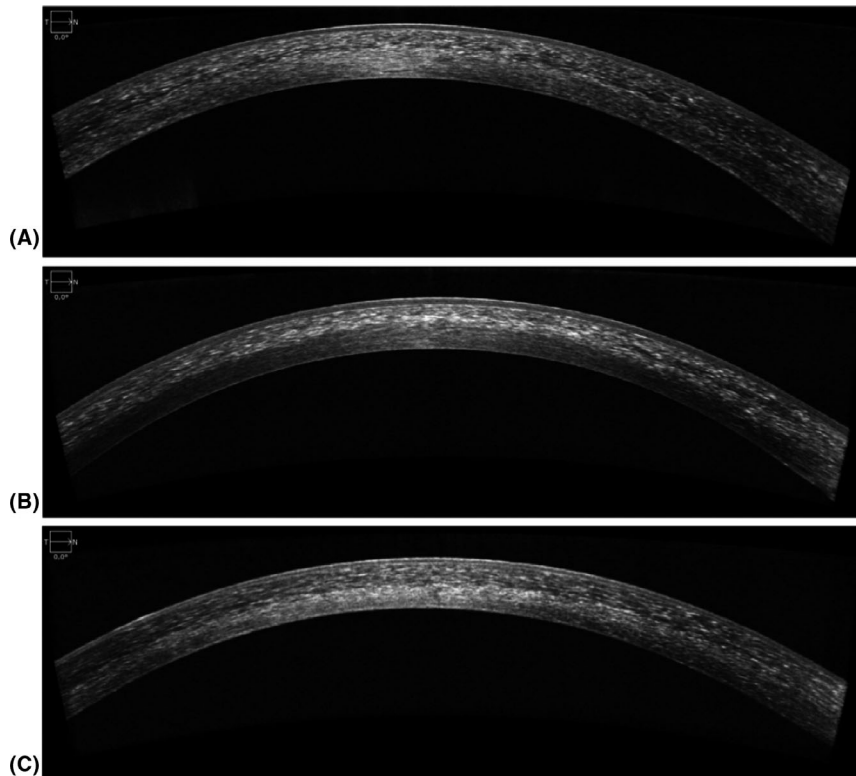


**Fig. 3.** Typical examples of corneal crystal deposition patterns: (A) crystals were distributed either in all stromal layers, (B) confined to the anterior or (C) posterior stroma, respectively.

**Table 2.** Digital calliper measurements and interrater correlations.

	Examiner 1	Examiner 2	Mean	Pearson's correlation ( $R^2$ )
Central corneal thickness				
Cystinosis	537 ± 34 μm	534 ± 36 μm	536 ± 35 μm	0.95
Healthy controls	517 ± 35 μm	514 ± 33 μm	516 ± 33 μm	0.84
Central stromal thickness				
Cystinosis	474 ± 35 μm	470 ± 35 μm	472 ± 34 μm	0.94
Healthy controls	450 ± 33 μm	456 ± 30 μm	453 ± 31 μm	0.81
Crystal depth distribution				
Posterior to Bowman's	378 ± 138 μm	360 ± 134 μm	369 ± 133 μm	0.86
% of stromal thickness	79 ± 28%	76 ± 27%	78 ± 27%	0.84

comparably favourable inter-rater correlation in healthy and cystinosis patients (Table 2). Central corneal ( $p < 0.001$ ) and stromal thickness ( $p < 0.001$ ) was significantly higher in cystinosis patients as compared with healthy controls. The depth of crystal deposits in the stroma reached a mean of  $369 \pm 133 \mu\text{m}$  below Bowman's membrane accounting for  $78 \pm 27\%$  of affected stromal depth. The depth of stromal crystal deposits increased significantly ( $p < 0.001$  in all comparisons) with age when compared to the youngest age group (Fig. 4). In all patients of the oldest subgroup

(>30a), crystal distribution affected virtually all corneal stromal layers.

**Objective, semi-automated AS-OCT image segmentation**

The three highest tested grey scale threshold values (211, 226 and 241) were the only thresholds that yielded statistically significant higher counts of suprathreshold pixels in cystinosis patients as compared to healthy controls (with  $p = 0.038$ ,  $p = 0.001$  and  $p < 0.001$ , respectively; Fig. 5). Examples of automated crystal delineation using the three respective threshold

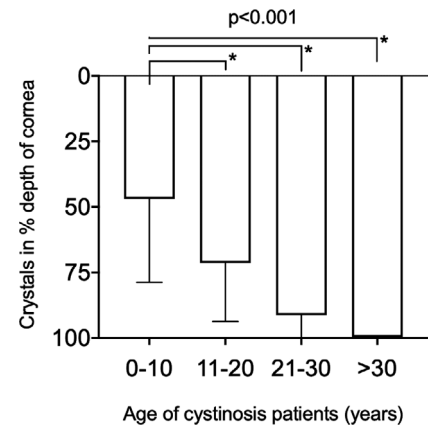


**Fig. 4.** Age dependence of crystal depth distribution. Depth of crystals as determined by the digital calliper method increased with age.

values are depicted in Fig. 6. The depth distributions of the suprathreshold grey scale values are displayed in Fig. 7. As with manual calliper measurements, the accumulation of crystals in the mid and posterior ROI segments increased with age (Fig. 7). In patients of 10 years or younger, 93% of detected crystals manifested in the anterior stromal segment and the remaining 7% in the mid ROI segment. In the oldest subgroup of >30 years, 50% of detected crystals fell into the mid or posterior segments.

**Correlation with visual acuity**

Best-correlated distance visual acuity showed no significant correlation with the numbers of pixels in % of the total ROI for the tested grey scale threshold values 211 ( $r = -0.046$ ;  $p = 0.74$ ), 226 ( $r = 0.012$ ,  $p = 0.93$ ) and 241 ( $r = -0.047$ ,  $p = 0.73$ ), respectively.

**Discussion**

Infantile nephropathic cystinosis has an estimated incidence of 1:100 000–1:200 000. (Elmonem et al. 2016). In Germany, approximately 130 patients are currently known and 3–5 new patients are diagnosed per year (Hohenfellner et al. 2019). Therefore, this comprehensively studied cohort of cystinosis patients may be regarded as highly valuable to broaden our understanding of this rare genetic disorder.

The main visual burden of cystinosis patients is related to cystine crystal deposition in various ocular structures. Corneal cystine crystal deposition predominantly in the corneal stroma

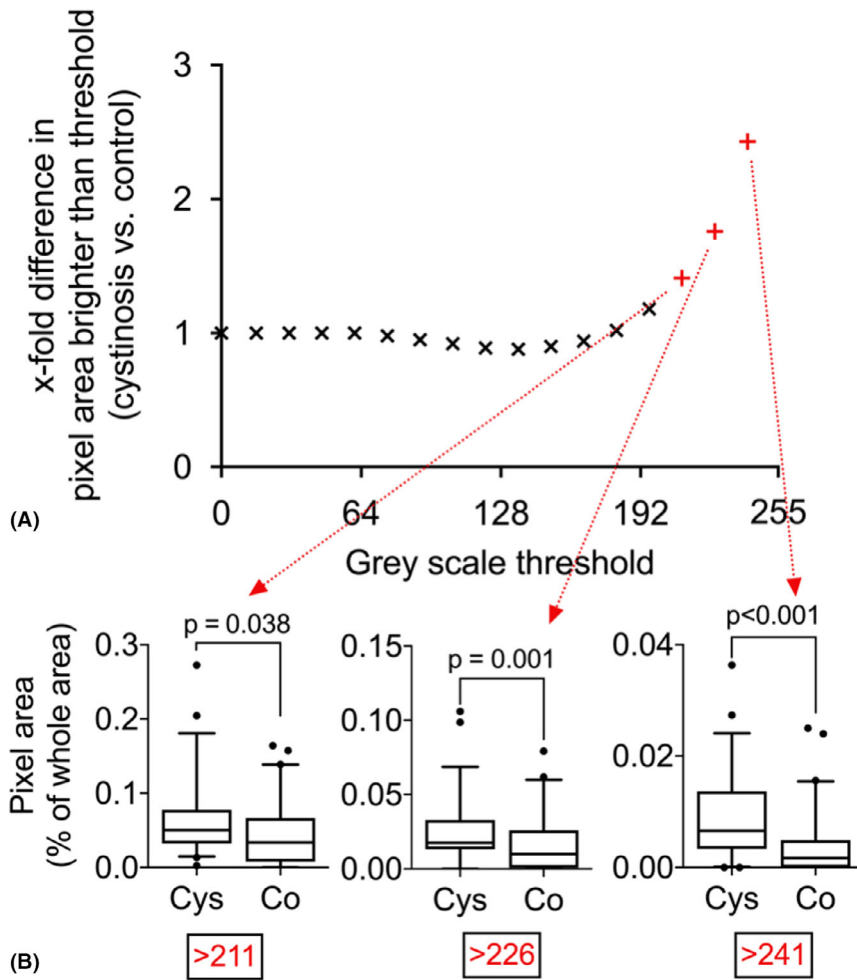


**Fig. 5.** (A) Scatter plot showing the x-fold difference of suprathreshold pixels between cystinosis patients and healthy controls using 16 different grey scale threshold values. (B) The three highest tested threshold values were the only thresholds to exhibit statistically significant differences in detected suprathreshold pixels between cystinosis patients and healthy controls.

causes severe photophobia and blepharospasm, thereby dramatically compromising patients' quality of life (Gahl et al. 2000). Especially in paediatric cystinosis but also in adult patients, monitoring of corneal cystine deposition is important to ensure adherence to topical cysteamine therapy, which has significant impact on disease progression (Gahl et al. 2000; Simpson et al. 2011a; Simpson et al. 2011b). As also confirmed in the present study, visual acuity must not be used as a biomarker for corneal disease as it correlates poorly with corneal crystal accumulation (Gahl et al. 1988; Biswas et al. 2018). Hence, ophthalmologists should rely on other clinical biomarkers of corneal involvement in cystinosis. As of today, three grading systems for corneal crystal deposition are available that depend on different imaging modalities: the clinical Gahl

slit lamp grading score based on slit lamp photography (Gahl et al. 2000), AS-OCT grading using a digital manual calliper to determine crystal depth distribution as well as the Labbé IVCN score evaluating crystal deposition semiquantitatively by comparing crystals with a standardized library of IVCN images (Labbe et al. 2009). Both slit lamp microscopy and IVCN operate in the visible light spectrum and, hence, are not suitable for most cystinosis patients, who suffer from severe photophobia. Moreover, IVCN is not widely clinically available, requires an experienced operator due to its contact and time-consuming nature, and its feasibility is limited in paediatric patients. Furthermore, neither the Gahl nor the Labbé score nor the application of callipers in AS-OCT represents objective measures of corneal crystal deposition and, thus, may

be prone to inter-investigator variability.

High-resolution AS-OCT overcomes many shortcomings of the aforementioned imaging techniques as it is a noncontact technique that operates in the infrared spectrum invisible for the human eye. In the present study, we developed and validated a semi-automated AS-OCT B-scan image segmentation algorithm to quantify corneal cystine crystal deposition. This methodology enables objective, operator- and patient-friendly measurements and, thus, has the potential to serve as a valuable biomarker for monitoring and treatment surveillance of the ocular manifestations in nephropathic cystinosis.

The novel semi-automated B-scan analysis algorithm developed in the present study allowed efficient and objective quantification and depth characterization of cornea crystal deposition. Both the digital calliper measurements employed in the present study as well as the novel AS-OCT imaging algorithm confirmed an evolution of cystin crystal deposition beginning in the anterior stroma in younger patients and incremental involvement of the mid and posterior stroma with increasing age. These findings are in concordance with previous slit lamp biomicroscopy observations (Melles et al. 1987; Dureau et al. 2003; Simpson et al. 2011a; Simpson et al. 2011b). Moreover, our study is the first to consider that the distribution patterns of corneal crystals appear too heterogeneous on AS-OCT to be evaluated by drawing digital callipers from the anterior corneal surface to judge crystal accumulation depth (Labbe et al. 2009). For instance, one quarter of eyes evaluated in the present study exhibited crystal deposits only in the anterior stroma whereas a further quarter showed crystals predominantly in the posterior stroma with marginal involvement of anterior layers. Whether these different patterns of crystal accumulation are related to disease duration itself, to the administration of cysteamine therapy or to other factors (e.g. the severity of cystinosis nephropathy) is still to be determined in future investigations. The standardized methodology developed in the present study may thereby broaden our understanding of the pathophysiology of corneal cystinosis.



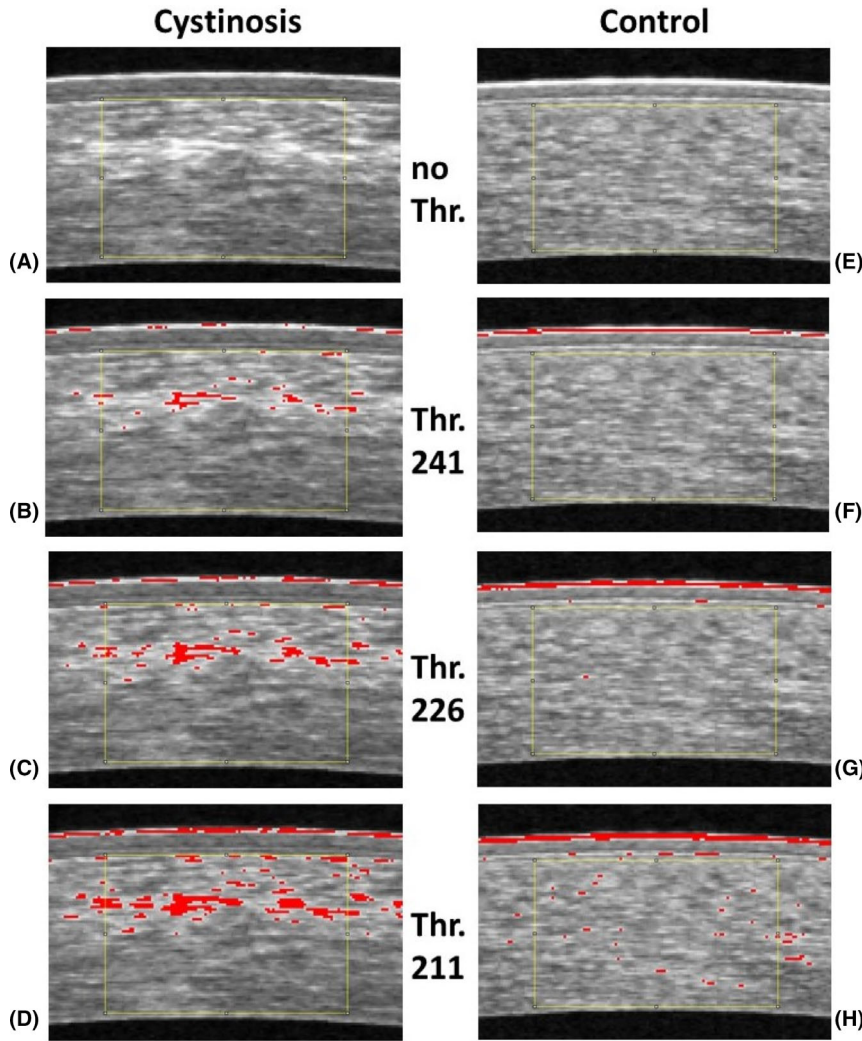


**Fig. 6.** Automated marking of corneal crystals presenting as hyperreflective foci in the OCT B-scan images. As seen in comparison to (A) no marking, the higher thresholds of (B) 241, (C) 226 and (D) 211 were able to yield an acceptable marking of crystal density. (E–H) Corneas of healthy control with the identical thresholds applied.

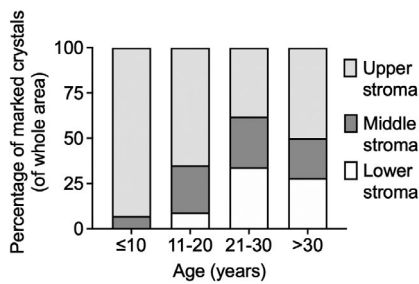


**Fig. 7.** Stromal depth distributions of automatically detected cystine crystals in different age groups.

In future longitudinal studies (e.g. that gauge the efficacy of novel therapeutic agents for corneal cystinosis), the number of pixels above the respective threshold as percentage of the pixel count in the whole ROI should be used

as a biomarker. As threshold 211 represents the lowest of the three thresholds that yielded statistically significantly higher counts of suprathreshold pixels in cystinosis patients as compared to healthy controls, we advocate using this threshold value in future studies. It shows the least probability to miss hyperreflective deposits (representative of cystine crystals) and still precisely demarcates normal tissue from cystine crystals (Fig. 6). Furthermore, the authors believe that this novel AS-OCT derived biomarker may also improve topical cysteamine therapy compliance, especially in paediatric patients. Both objectively quantifying and visualizing therapeutic success in form of a regression of corneal crystal deposition (e.g. graphically displayed with colour-coded AS-

OCT B-scan images) may be highly motivational for patients to adhere to their therapy regimen. Moreover, topical therapy regimens may be individually titrated according to corneal crystal deposition patterns or densities.

Limitations to this study may be found. First and foremost, the study is limited by its cross-sectional nature. A longitudinal study investigating the effects of topical and systemic therapy on corneal cystinosis disease severity and progression is to be initiated based on the findings of the present study. Moreover, as cystinosis is considered an orphan disease with extremely low prevalence, the small sample size analysed in the present is naturally limited. As a technical limitation related to the OCT system, only one singular B-scan image was analysed in the present study. In future studies, ideally, a high acquisition speed OCT system with a very dense radial scanning pattern enabling 3-dimensional renderings of cystine crystals should be employed.

To conclude, the novel AS-OCT based imaging algorithm enables for the first time to not only objectively quantify stromal crystal density but also to characterize different depth distribution patterns in corneal cystinosis. This contact-free and easy to use imaging technique may aid in improving physicians' and patients' understanding of the disease's pathophysiology and foster therapy adherence. Moreover, AS-OCT based corneal crystal quantification may serve as an objective biomarker in future clinical studies evaluating novel therapeutic approaches to prevent or reverse corneal crystal deposition.

## References

- Biswas S, Gaviria M, Malheiro L, Marques JP, Giordano V & Liang H (2018): Latest clinical approaches in the ocular management of cystinosis: a review of current practice and opinion from the ophthalmology cystinosis forum. *Ophthalmol Ther* 7: 307–322.
- Blanksma LJ, Jansonius NM & Reitsma-Bierens WC (1996): Cysteamine eyedrops in three patients with nephropathic cystinosis. *Doc Ophthalmol* 92: 51–53.
- Bradbury JA, Danjoux JP, Voller J, Spencer M & Brocklebank T (1991): A randomised placebo-controlled trial of topical cysteamine therapy in patients with nephropathic cystinosis. *Eye (Lond)* 5(Pt 6): 755–760.

- Cantani A, Giardini O & Ciarella Cantani A (1983): Nephropathic cystinosis: ineffectiveness of cysteamine therapy for ocular changes. *Am J Ophthalmol* **95**: 713–714.
- David D, Princiero Berlingero S, Elmonem MA, Oliveira Arcolino F, Soliman N, van den Heuvel B, Gijsbers R & Levchenko E (2019): Molecular basis of cystinosis: geographic distribution, functional consequences of mutations in the CTNS gene, and potential for repair. *Nephron* **141**: 133–146.
- Dureau P, Broyer M & Dufier JL (2003): Evolution of ocular manifestations in nephropathic cystinosis: a long-term study of a population treated with cysteamine. *J Pediatr Ophthalmol Strabismus* **40**: 142–146.
- Elmonem MA, Veys KR, Soliman NA, van Dyck M, van den Heuvel LP & Levchenko E (2016): Cystinosis: a review. *Orphanet J Rare Dis* **11**: 47.
- Gahl WA, Bashan N, Tietze F, Bernardini I & Schulman JD (1982): Cystine transport is defective in isolated leukocyte lysosomes from patients with cystinosis. *Science* **217**: 1263–1265.
- Gahl WA, Reed GF, Thoene JG et al. (1987): Cysteamine therapy for children with nephropathic cystinosis. *N Engl J Med* **316**: 971–977.
- Gahl WA, Thoene JG, Schneider JA, O'Regan S, Kaiser-Kupfer MI & Kuwabara T (1988): NIH conference. Cystinosis: progress in a prototypic disease. *Ann Intern Med* **109**: 557–569.
- Gahl WA, Charnas L, Markello TC, Bernardini I, Ishak KG & Dalakas MC (1992): Parenchymal organ cystine depletion with long-term cysteamine therapy. *Biochem Med Metab Biol* **48**: 275–285.
- Gahl WA, Kuehl EM, Iwata F, Lindblad A & Kaiser-Kupfer MI (2000): Corneal crystals in nephropathic cystinosis: natural history and treatment with cysteamine eyedrops. *Mol Genet Metab* **71**: 100–120.
- Gahl WA, Thoene JG & Schneider JA (2002): Cystinosis. *N Engl J Med* **347**: 111–121.
- Graf M, Grote A & Wagner F (1992): Cysteamine eyedrops for treatment of corneal cysteine deposits in infantile cystinosis. *Klin Monbl Augenheilkd* **201**: 48–50.
- Han SB, Liu YC, Noriega KM & Mehta JS (2016): Applications of anterior segment optical coherence tomography in cornea and ocular surface diseases. *J Ophthalmol* **2016**: 4971572.
- Hohenfellner K, Bergmann C, Fleige T et al. (2019): Molecular based newborn screening in Germany: follow-up for cystinosis. *Mol Genet Metab Rep* **21**: 100514.
- Jones NP, Postlethwaite RJ & Noble JL (1991): Clearance of corneal crystals in nephropathic cystinosis by topical cysteamine 0.5%. *Br J Ophthalmol* **75**: 311–312.
- Kaiser-Kupfer MI, Caruso RC, Minkler DS & Gahl WA (1986): Long-term ocular manifestations in nephropathic cystinosis. *Arch Ophthalmol* **104**: 706–711.
- Kaiser-Kupfer MI, Fujikawa L, Kuwabara T, Jain S & Gahl WA (1987): Removal of corneal crystals by topical cysteamine in nephropathic cystinosis. *N Engl J Med* **316**: 775–779.
- Kalatzis V & Antignac C (2003): New aspects of the pathogenesis of cystinosis. *Pediatr Nephrol* **18**: 207–215.
- Kalatzis V, Serratrice N, Hippert C et al. (2007): The ocular anomalies in a cystinosis animal model mimic disease pathogenesis. *Pediatr Res* **62**: 156–162.
- Labbe A, Niaudet P, Loirat C, Charbit M, Guest G & Baudouin C (2009): In vivo confocal microscopy and anterior segment optical coherence tomography analysis of the cornea in nephropathic cystinosis. *Ophthalmology* **116**: 870–876.
- Liang H, Baudouin C, Joutei Hassani RT, Brignole-Baudouin F & Labbe A (2015): Photophobia and corneal crystal density in nephropathic cystinosis: an in vivo confocal microscopy and anterior-segment optical coherence tomography study. *Invest Ophthalmol Vis Sci* **56**: 3218–3225.
- Melles RB, Schneider JA, Rao NA & Katz B (1987): Spatial and temporal sequence of corneal crystal deposition in nephropathic cystinosis. *Am J Ophthalmol* **104**: 598–604.
- Nesterova G & Gahl W (2008): Nephropathic cystinosis: late complications of a multisystemic disease. *Pediatr Nephrol* **23**: 863–878.
- Nesterova G & Gahl WA (2013): Cystinosis: the evolution of a treatable disease. *Pediatr Nephrol* **28**: 51–59.
- Simpson JL, Nien CJ, Flynn KJ & Jester JV (2011a): Evaluation of topical cysteamine therapy in the CTNS(-/-) knockout mouse using in vivo confocal microscopy. *Mol Vis* **17**: 2649–2654.
- Simpson J, Nien CJ, Flynn K, Jester B, Cherqui S & Jester J (2011b): Quantitative in vivo and ex vivo confocal microscopy analysis of corneal cystine crystals in the Ctns knockout mouse. *Mol Vis* **17**: 2212–2220.
- Thoene JG, Oshima RG, Crawhall JC, Olson DL & Schneider JA (1976): Cystinosis. Intracellular cystine depletion by aminothiois in vitro and in vivo. *J Clin Invest* **58**: 180–189.
- Town M, Jean G, Cherqui S et al. (1998): A novel gene encoding an integral membrane protein is mutated in nephropathic cystinosis. *Nat Genet* **18**: 319–324.
- Tsilou E, Zhou M, Gahl W, Sieving PC & Chan CC (2007): Ophthalmic manifestations and histopathology of infantile nephropathic cystinosis: report of a case and review of the literature. *Surv Ophthalmol* **52**: 97–105.

Received on February 19th, 2020.  
Accepted on July 2nd, 2020.

*Correspondence:*

Nikolaus Luft, MD, PhD, FEBO  
Claudia Priglinger, MD, FEBO  
Department of Ophthalmology  
Ludwig-Maximilians-University Munich  
Mathildenstraße 8  
80336 Munich, Germany  
Phone: +49 (0)89 4400-53811  
Fax: +49 (0)89 4400-55160  
Emails: claudia.priglinger@med.uni-muenchen.de (CP); nikolaus.luft@med.uni-muenchen.de (NL)

Leonie Keidel received previous speaker fees and/or travel expenses from Recordati Rare Diseases Inc. and Roche Diagnostics GmbH. Carolin Elhardt and Christian Wertheimer have no conflicts of interest to declare. Katharina Hohenfellner received previous speaker fees from Recordati Rare Diseases Inc. Benedikt Schworm received previous speaker fees and travel expenses from Novartis Pharma GmbH and Topcon Corporation. Nikolaus Luft received income from honoraria as a lecturer from Alcon Laboratories Inc., NIDEK Co. Ltd and CenterVue SpA. Claudia Priglinger received previous speaker fees from Novartis Pharma GmbH and travel expenses from Recordati Rare Diseases Inc.